Analytical and Bioanalytical Chemistry
https://doi.org/10.1007/s00216-024-05133-y

RESEARCH PAPER

Electrochemiluminescent imaging of a NADH-based enzymatic reaction confined within giant liposomes

Fatma Ben Trad[1] · Bixente Carré[1] · Jérôme Delacotte[1] · Frédéric Lemaître[1] · Manon Guille-Collignon[1] · Stéphane Arbault[2] · Neso Sojic[3] · Eric Labbé[1] · Olivier Buriez[1]

Received: 22 November 2023 / Revised: 21 December 2023 / Accepted: 8 January 2024

Abstract

Herein, transient releases either from NADH-loaded liposomes or enzymatic reactions confined in giant liposomes were imaged by electrochemiluminescence (ECL). NADH was first encapsulated with the $[Ru(bpy)_3]^{2+}$ luminophore inside giant liposomes (around 100 µm in diameter) made of DOPC/DOPG phospholipids (i.e., 1,2-dioleolyl-sn-glycero-3-phosphocholine/1,2-dioleoyl-sn-glycerol-3-phospho-(1′-rac-glycerol) sodium salt) on their inner- and outer-leaflet, respectively. Then, membrane permeabilization triggered upon contact between the liposome and a polarized ITO electrode surface and ECL was locally generated. Combination of amperometry, photoluminescence, and ECL provided a comprehensive monitoring of a single liposome opening and content release. In a second part, the work is focused on the ECL characterization of NADH produced by glucose dehydrogenase (GDH)-catalyzed oxidation of glucose in the confined environment delimited by the liposome membrane. This was achieved by encapsulating both the ECL and catalytic reagents (i.e., the GDH, glucose, NAD^+, and $[Ru(bpy)_3]^{2+}$) in the liposome. In accordance with the results obtained, NADH can be used as a biologically compatible ECL co-reactant to image membrane permeabilization events of giant liposomes. Under these conditions, the ECL signal duration was rather long (around 10 s). Since many enzymatic reactions involve the NADH/NAD^+ redox couple, this work opens up interesting prospects for the characterization of enzymatic reactions taking place notably in artificial cells and in confined environments.

Keywords Electrochemiluminescence · Imaging · Amperometry · NADH · Liposome · Release

Introduction

Given the ubiquity of the reduced form of nicotinamide adenine dinucleotide (NADH) in redox enzymatic reactions as well as the cell metabolism, addressing its detection and/or analysis, whether in vivo or in vitro, became a crucial issue. Due to the intrinsic luminescence and redox properties of NADH, most of approaches developed so far to detect it are mainly based on optical or electrochemical sensing.

On the one hand, the intrinsic fluorescence of NADH ($\lambda_{abs} = 340 \pm 30$ nm; $\lambda_{em} \sim 460 \pm 50$ nm) can be exploited to quantify and image NADH in living cells [1]. Nevertheless, its quantum yield is relatively poor, and its own fluorescence can interfere with cellular autofluorescence. To overcome these drawbacks, small molecule-based fluorescent probes [2, 3] or genetically encoded fluorescent sensors [4, 5] have been developed to monitor and image NADH in living cells and in vivo though the addition of external probes may disrupt samples. In parallel, biochemical analyses including

Published in the topical collection *Optical Biosensors and Biomimetic Sensors for Chemical Analysis* with guest editors Elena Benito-Peña and Guillermo Orellana.

In honor of Professor María Cruz Moreno Bondi.

✉ Neso Sojic
sojic@u-bordeaux.fr

✉ Olivier Buriez
olivier.buriez@ens.psl.eu

[1] PASTEUR, Département de Chimie, Ecole Normale Supérieure, PSL University, Sorbonne Université, CNRS, 75005 Paris, France

[2] Univ. Bordeaux, CNRS, Bordeaux INP, CBMN, UMR 5248, 33600 Pessac, France

[3] Univ. Bordeaux, CNRS, Bordeaux INP, ISM, UMR 5255 CNRS, 33400 Talence, France

Published online: 16 January 2024

capillary electrophoresis [6], high-performance liquid chromatography [7], colorimetry [8], or enzymatic cycling assays [9] allow detecting NADH in vitro. Although optical approaches, based on absorbance or fluorescence, provide both high sensitivity and excellent spatial resolutions, they may however lack the temporal resolution notably in in vitro experiments.

On the other hand, the redox properties of NADH have also contributed to the development of various electrochemical approaches to detect it, especially in vitro, with the advantage of access to excellent temporal resolutions (rapid response time), small sampling volume and cost-effective protocols [10, 11]. However, the direct oxidation of NADH at bare electrodes is not so straight since strongly depending on experimental conditions (nature of the electrode material, buffer composition, pH, ionic strength, temperature, scan rate, etc.) [12]. This led to the modification of electrode surfaces with (i) a variety of molecular redox mediators (e.g., quinone derivatives, phenazine) catalyzing the NADH oxidation [13–15], (ii) polymers [16, 17], or (iii) nanomaterials (carbon nanotubes, graphene sheets) [18, 19].

Within this framework, considering both advantages brought by luminescence and electrochemistry in terms of spatial and temporal resolutions, respectively (additionally to their respective high sensitivity), the development of approaches based on electrochemiluminescence (ECL) to detect and/or analyze NADH in micro-volumes or confined environments appears therefore as a good compromise.

ECL, also called electrogenerated chemiluminescence, is a light-emitting phenomenon triggered by an initial electrochemical reaction. On the one hand, an electron transfer occurring at an electrode surface allows generation of the excited state of a luminophore. On the other hand, the optical signal comes from the emitted photons during the relaxation of the luminophore excited state. Accordingly, and compared to fluorescence-based approaches, the absence of incident light leads to a very high sensitivity and gives therefore access to a wide range of analytes [20, 21]. The ECL approach is nowadays recognized as a powerful analytical method for immunoassays and clinical diagnosis [22–26]. Moreover, the fact that ECL does not require any irradiation (suppressing thus related inherent issues such as photobleaching, photo-blinking, background scattered light, cell phototoxicity, or sample autofluorescence) led this method to evolve towards a microscopy technique [27–29]. Taking advantage of both advances in microscopic analysis equipment and the emergence of a variety of nanomaterials [30], ECL imaging is being increasingly used as an approach to visualize single objects [31–34], especially of biological interest [35–46].

In this context, though the direct detection of NADH has been successfully achieved by ECL [47–55], only few articles focus on its ECL imaging [56–58], most likely because the development of new and sensitive microscopic analyses is fairly recent. In these examples, NADH was detected either through an ordered array of nanoapertures [56], in paper-based microfluidic sensors [57], or at a Nafion-modified fiber electrode [58], the enzymatic cofactor acting as a co-reactant while $[Ru(bpy)_3]^{2+}$ was the luminophore. Similarly, few NADH-centered ECL works devoted to the detection of enzymatically formed analytes [59–66] go as far as imaging the ECL response. Interestingly, most of these works were performed either under bulk conditions or in the presence of electrodes modified with a variety of matrix immobilizing ECL reagents and/or enzymes for sensitivity reasons. Surprisingly, the detection or analysis of NADH trapped or enzymatically generated in confined bio-architectures like liposomes has, to the best of our knowledge, never been investigated. Yet, liposomes and notably giant unilamellar vesicles (GUVs) represent a simple and manageable cell-mimetic system [67] that can be easily manipulated and visualized by optical microscopy techniques [68–72].

Recently, we developed an original ECL approach allowing the membrane permeabilization imaging of giant liposomes (100 µm in diameter) triggered either by a polarized electrode surface [73] or by melittin, an antimicrobial peptide known to make pores in phospholipid membranes [74]. In both cases, the luminophore $[Ru(bpy)_3]^{2+}$ was used in combination with tri-*n*-propylamine (TPrA) as the sacrificial co-reactant. This approach remains hampered by the low biocompatibility of the high concentration of TPrA co-reactant used especially when working with liposomes, the archetypal model cells. It would be therefore interesting to substitute TPrA by a more biocompatible and relevant co-reactant like NADH that can promote ECL thanks to its aliphatic tertiary amine group. Indeed, the oxidized form of the co-enzyme, NAD^+, does not generate ECL because the aromatic amines (such as the pyridine ring of NAD^+) are known to do not undergo ECL emission with $[Ru(bpy)_3]^{2+}$. In NADH, the aromaticity of the pyridine ring can no longer take place and the tertiary amine group produces ECL signal. Herein, it is shown that (i) authentic NADH can be used as an ECL co-reactant to image the membrane permeabilization of liposomes triggered by the polarization of the electrode surface on which they are lying and (ii) NADH-promoted ECL can image the glucose dehydrogenase (GDH) activity in the confined environment delimited by the liposome architecture. This was achieved by encapsulating in giant liposomes both enzymatic and ECL reagents (Fig. 1).

Experimental section

Reagents All the reagents were purchased from Sigma-Aldrich unless otherwise noted. The following lipids were purchased from Avanti Polar Lipids:

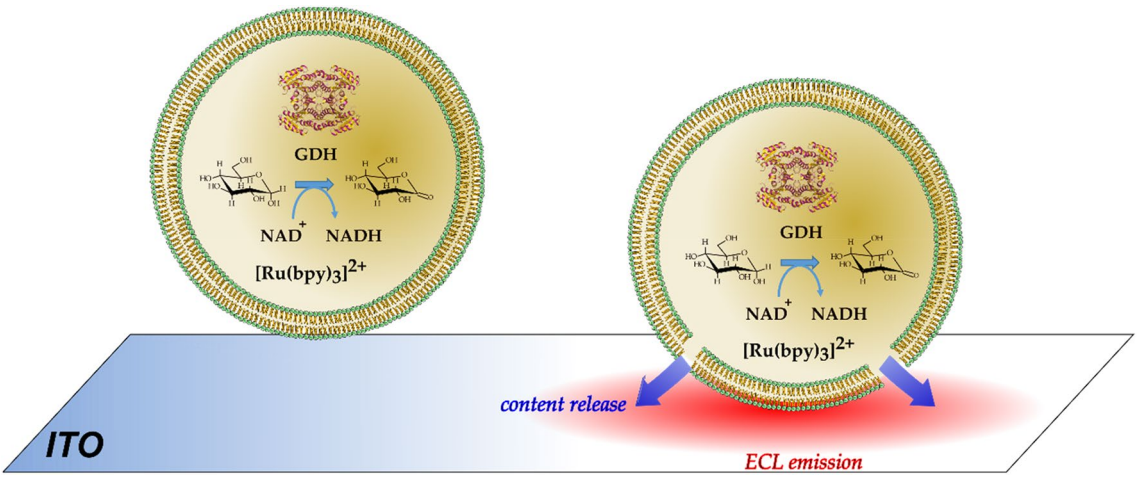

Fig. 1 ECL imaging of the transient release by a liposome in which GDH catalyzes the oxidation of glucose concomitantly with the reduction of NAD^+ to NADH. ECL emission from the $[Ru(bpy)_3]^{2+}$ luminophore occurs at the ITO electrode surface upon the opening of the liposome

1,2-dioleoyl-sn-glycerol-3-phospho-(1′-*rac*-glycerol) sodium salt (DOPG, 10 mg/mL in chloroform) and 1,2-dioleolyl-sn-glycero-3-phosphocholine (DOPC, 10 mg mL^{-1} in chloroform). All chemicals were used as received.

Extra- and intra-vesicular solutions were prepared with a highly purified water (resistivity = 18 MΩ cm; Milli-Q system; Millipore, Billerica, MA, USA). The extravesicular solution was prepared by dissolving glucose in PBS to obtain a concentration of 0.7 M and an osmolality of ~ 1000 mOsm kg^{-1}. The intra-vesicular solution contained a mixture of sucrose at 0.7 mol L^{-1} and glucose at 0.7 mol L^{-1} (v/v = 50/50) in PBS, $[Ru(bpy)_3]^{2+}$ at 250 µmol L^{-1}, NADH (or NAD^+) at 10 mmol L^{-1}, and GDH at 80 U/mL. This solution also had an osmolality of ~ 1000 mOsm kg^{-1}. Importantly, the 7.4 pH value was adjusted by addition of phosphoric acid. The osmolality had to be sometimes adjusted by adding small amounts of the PBS solution to ensure isotonic conditions.

Phospholipids in oil suspensions were made as follows: first, DOPG or DOPC (121 µL; 10 mg/mL in chloroform) was added in a 2-mL glass vial to evaporate chloroform under vacuum (2 h). Then, mineral oil (2 mL) was added to dried phospholipids and the corresponding suspension was sonicated (1 h).

Instrumentation The ECL experiments have been performed with a µAUTOLAB Type III and an inverted Zeiss Observer.Z1 microscope equipped with an EMCCD camera (C9100-13, Hamamatsu, Japan). The microscope was inside a Faraday cage. Photoluminescence (PL) excitation was performed with a diode (THORLABS M455L3, λ_{ex} = 455 nm). The $[Ru(bpy)_3]^{2+}$ luminophore was illuminated with a Zeiss filter set 74HE. Cyclic voltammograms were recorded with an Autolab potentiostat (PGSTAT 20).

$[Ru(bpy)_3]^{2+}$/NADH encapsulated giant liposomes The preparation of giant liposomes was performed through two successive steps as detailed in a previous work [73]. Encapsulation of ECL reagents (ruthenium complex as well as NADH or NAD^+/GDH) was achieved during the first step corresponding to the formation of water in oil droplets.

Imaging of GUVs The giant liposomes lying on the ITO electrode were imaged by fluorescence microscopy (Zeiss Observer.Z1), using N-Achroplan 10× (aperture 0.25) and LD Plan-Neofluar 20× (numerical aperture 0.6) objectives. Fluorescence excitation was provided by a mercury lamp (HXP 120C) and by selecting the right filter to evidence NADH (Zeiss filter set 49, λ_{ex} = 365 nm and λ_{em} = 450 nm). During the ECL imaging, PL images were recorded concomitantly by illumination with a flashing diode (THORLABS M455L3, λ_{ex} = 455 nm).

ITO microelectrodes The ITO microelectrodes were fabricated from optical glass slides (22 mm × 22 mm × 0.13 mm) coated with 150-nm-thick ITO films (90% In_2O_3/10% SnO_2, ACM, Villiers Saint Frédéric, France). The ITO electrode surface (~ 800 µm in diameter) was delimited by a PDMS well in which a 1-mL micropipette tip, playing the role of the electrochemical cell, was inserted vertically to the glass surface. A detailed description was reported in reference [73].

Combination of ECL/PL experiments The ECL and PL experiments were performed simultaneously with a µAUTOLAB Type III and through an e-corder 401 system (eDAQ Pty Ltd, Australia) associated with the eDAQ Chart software. The ECL images were collected by an inverted Zeiss LSM 710 microscope equipped with an EMCCD camera (Hamamatsu, Japan). It was located inside a Faraday cage. A constant

potential of + 1.2 V vs. Ag/AgCl was imposed to the ITO working electrode. A platinum wire was the counter electrode. Images were registered and treated by using HCImage Live and ImageJ softwares, respectively. The appropriate time sequences for the combined detection of ECL and PL signals are given in Figure S5 of the Electronic Supplementary Material.

Results and discussion

ECL imaging of a liposome opening loaded with authentic NADH as the co-reactant

In a recent study, the permeabilization of liposomes containing $[Ru(bpy)_3]^{2+}$ and TPrA has been reported via the ECL signal produced through the concomitant oxidation of the luminophore and co-reactant at an ITO electrode [73, 74]. This ECL imaging approach has been transposed in this work to NADH-promoted ECL, in order to monitor the release of liposomes acting as enzymatic reactors [60, 62, 75, 76].

Asymmetric DOPC/DOPG (inner-/outer-leaflet with neutral and negative charge, respectively) giant liposomes (100 µm in diameter) were first successfully loaded with the ruthenium complex (0.25×10^{-3} mol L^{-1}) and authentic NADH (10^{-2} mol L^{-1}) during their formation process. Liposomes were then deposited at the top of a homemade electrochemical cell, allowing them to sediment on the surface of an ITO electrode set at a potential value of + 1.2 V vs. Ag/AgCl (see Electronic Supplementary Material Fig. S1). This polarization is expected to destabilize the membrane due to a charge effect and allows permeabilization of the liposomes. Such a leakage consequently releases the ECL reagents in the extravesicular medium and their electrochemical oxidation leads to the corresponding amperometric signal as a function of time [73]. In addition, we selected this potential because it has been reported that ECL is initiated only at sufficiently positive potentials where $[Ru(bpy)_3]^{2+}$ is oxidized [56]. This was also confirmed by controlled experiments in which the ECL reagents (i.e., the ruthenium complex and NADH or NAD^+/GDH mixture) were in bulk solution (i.e., not encapsulated inside liposomes — see Electronic Supplementary Material Figs. S2 and S3). The ECL mechanism with NADH co-reactant can be described by successive reactions, which follow an oxidative-reductive scheme:

$$NADH \rightarrow NADH^{\bullet+} + e^- \quad (1)$$

$$[Ru(bpy)_3]^{2+} \rightarrow [Ru(bpy)_3]^{3+} + e^- \quad (2)$$

$$[Ru(bpy)_3]^{3+} + NADH \rightarrow [Ru(bpy)_3]^{2+} + NADH^{\bullet+} \quad (3)$$

$$NADH^{\bullet+} \rightarrow NAD^{\bullet} + H^+ \quad (4)$$

$$[Ru(bpy)_3]^{3+} + NAD^{\bullet} \rightarrow [Ru(bpy)_3]^{2+*} + NAD^+ \quad (5)$$

$$[Ru(bpy)_3]^{2+*} \rightarrow [Ru(bpy)_3]^{2+} + h\nu_{ECL} \quad (6)$$

The combination of amperometry with both ECL and photoluminescence (PL) imaging to visualize the spatial opening/rupture of liposomes and the corresponding release of their content into the extravesicular medium was achieved with a microscope equipped with an EMCCD camera (see Electronic Supplementary Material Fig. S4). Since a single camera can be combined with the microscope device to register the two different types of luminescent signal (ECL and PL), a diode ($\lambda_{ex} = 455$ nm) was set in a flashing mode to better distinguish both signals. Thus, ECL and PL images could be recorded separately and then reassembled to build two series of ECL and PL images as a function of time. The appropriate time sequences for the combined detection of amperometry, ECL, and PL signals are shown in Figure S5 (see Electronic Supplementary Material). Figure 2 displays two sets of images obtained in ECL and PL (Fig. 2a) together with the corresponding intensity profiles of the amperometric, PL, and ECL signals (Fig. 2b).

The PL images show the presence of two vesicles close to each other (see images taken at $t = 64$ and 65 s). Before $t \leq 65$ s, no ECL signal was visible, indicating the absence of detectable leakage from the liposomes observed in PL. Then, from $t = 68$ s, an arc-shaped ECL signal appeared at the liposome close to the left in the image. At the same time, the light intensity emitted by this liposome in PL became diffuse and concomitantly decreased. This event, observed sequentially in both PL and ECL modes over the same time window, unambiguously indicates a liposome leakage. As already reported with TPrA, no ECL signal was emitted at the liposome-electrode contact point, accounting for the absence of electron transfer across the lipid bilayer [73]. Accordingly, the ECL signal can be observed beyond the blocked area thanks to a convective regime triggered by the brutal rupture of the liposome.

In order to better rationalize such a permeabilization event, a region of interest (ROI) was first defined around the investigated liposome. Then, the corresponding ECL, PL, and current magnitudes were plotted as a function of time (Fig. 2b). Accordingly, for $0 < t < 60$ s, PL displays the only observable/significant signal in the time window. In particular, the increase in PL signal intensity between $t = 15$ and $t = 20$ s corresponds to the sedimentation of the liposome at the electrode surface (the microscope observation was focused at the ITO electrode surface). Then, the liposome begins to leak between $t = 65$ and 68 s, leading to a sharp drop in the PL signal, the intensity of which being

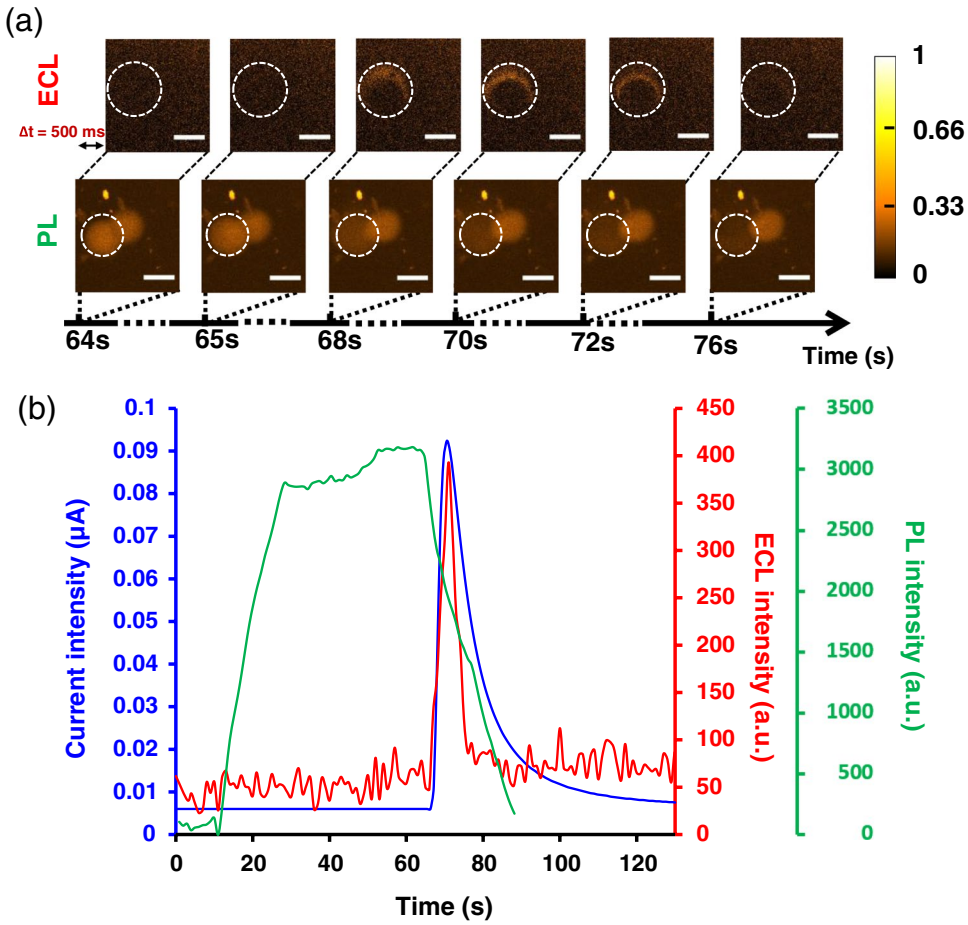

Fig. 2 **a** Parallel timelapse imaging by ECL (top) and PL (below) showing the permeabilization of a DOPC/DOPG liposome in contact with a polarized ITO electrode surface (+1.2 V vs. Ag/AgCl). The liposome initially contains NADH (10^{-2} mol L^{-1}) and $[Ru(bpy)_3]^{2+}$ (2.5×10^{-4} mol L^{-1}). To avoid overlapping between the two signals, ECL and PL images have been recorded with an initial image acquisition time delay (Δt) of 500 ms. The focus was made at the ITO electrode surface during the ECL and PL imaging. The dotted white circles in PL and ECL images represent the region of interest (ROI) taken into account for the quantitative analyses of the corresponding intensities. Scale bar: 100 µm. **b** Evolution of PL (green curve), ECL (red curve), and amperometric current (blue curve) signals obtained as a function of time for a single liposome (shown in the ROI of **a**). Note: $t = 0$ s corresponds to the addition of liposomes in the electrochemical cell

proportional to the luminophore concentration. In the same time range, the ECL intensity and amperometric current increase very rapidly, in line with the oxidation of reagents leaking from the liposome.

Interestingly, the ECL signal duration was large (around 10 s) but it decreased faster than the current intensity profile that mostly accounts for the NADH oxidation (40 times more concentrated than the ruthenium complex). In agreement with our previous investigations [73], this would be due to convection produced by the brutal liposome opening, affecting the motion of the ruthenium luminophore and its fast local dilution. It is important to keep in mind that both ECL reagents have to be oxidized at the electrode surface, but that only the excited state of $[Ru(bpy)_3]^{2+}$ generates the ECL light.

ECL imaging to detect enzymatically produced NADH inside a giant liposome

In a second series of studies, we aimed at pushing the limits of this ECL-based approach to image the production of NADH resulting from an enzymatic reaction occurring inside a liposome used as a micro-reactor. We selected the GDH, which catalyzes the oxidation of glucose. Compared to the experiments described in the previous paragraph, the oxidized ECL-silent form of the co-enzyme ($[NAD^+] = 10^{-2}$ mol L^{-1}) was introduced into the liposome. To convert NAD^+ to NADH, the GDH (80 U/mL) and glucose (0.35 mol L^{-1}) were also loaded inside liposomes in addition to the ruthenium complex ($0.25 \cdot 10^{-3}$ mol L^{-1}) and sucrose (0.35 mol L^{-1}), the latter allowing sedimentation of the liposomes. Importantly, and as confirmed by cyclic voltammetry, the time required to obtain a maximum amount of NADH under our experimental conditions (around 1 h — see Electronic Supplementary Material Fig. S6) was similar to that needed to prepare liposomes. Photoluminescence microscopy images recorded 1 h after liposome preparation confirmed the encapsulation of enzymatically produced NADH inside the liposomes (Fig. 3). As shown in Fig. 3, NADH was homogeneously distributed inside the liposomes, similarly to the ruthenium complex observed at the start of liposomes preparation (compare Fig. 3 a and b).

Then, intact liposomes, like the one shown in Fig. 3, were dropped at the top of the electrochemical cell to image by ECL and PL their permeabilization upon impact with the polarized ITO electrode. Figure 4 depicts two series of ECL

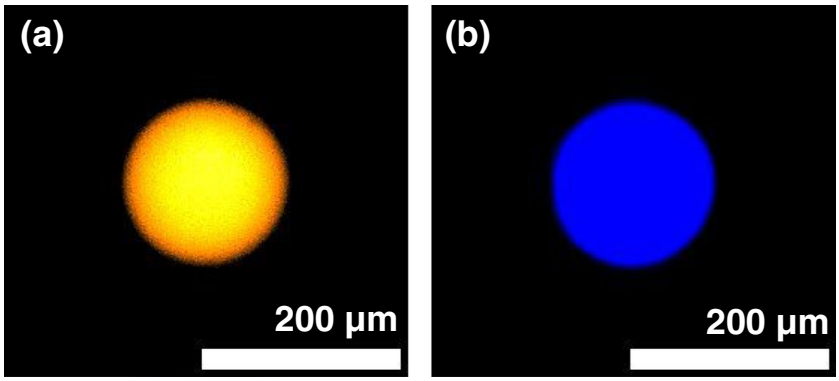

Fig. 3 PL images of **a** $[Ru(bpy)_3]^{2+}$ and **b** NADH within the same single liposome. Microscopy images of giant asymmetrical liposomes made of DOPC (neutral) and DOPG (negatively charged) on their outer- and inner-leaflet, respectively. In **a**, the liposome contains $[Ru(bpy)_3]^{2+}$ (C = 2.5 10^{-4} mol L^{-1}), NAD^+ (10^{-2} mol L^{-1}), GDH (80 U/mL), glucose (0.35 mol L^{-1}), and sucrose (0.35 mol L^{-1}) dissolved in PBS (10^{-2} mol L^{-1}, pH = 7.5). The images (**a**: λ_{ex} = 550 nm; λ_{em} = 605 nm for $[Ru(bpy)_3]^{2+}$ image and **b**: λ_{ex} = 365 nm; λ_{em} = 445 nm for NADH image) were obtained 1 h after starting the liposome preparation

and PL images as well as the corresponding quantitative ECL, PL, and current intensities determined from the ROI described by the white dashed circle.

Among several liposomes observed in the time window starting at $t = 14$ s and ending at $t = 52$ s (Fig. 4a), only the one positioned at the bottom center of the image appeared to be relevant in terms of permeabilization (liposome circled by a dotted line in Fig. 4a). As shown in Fig. 4a, this liposome is indeed the only one to undergo the effects of polarization. The fact that other liposomes are not affected by polarization can be explained by (i) a lack of direct contact with the electrode surface, (ii) an electrode surface defect or surface fouling, (iii) an increased membrane stability due to the absence of membrane defects, etc.

For $t < 24$ s, this liposome appears intact in PL. Besides, no ECL signal appears in this time range. In contrast, PL images recorded from 24 s time show the liposome deformation coupled with light scattering in the space near the vesicle. In the same time range, a signal (at the bottom of the images) appears on the ECL images, whose intensity decreases over time (compared to the 3 ECL images recorded between 24 and 52 s). On the one hand, the observations made in PL show that the liposome undergoes membrane leakage/permeabilization. On the other hand, the ECL signal unambiguously indicates that NADH has indeed been formed by enzymatic oxidation of glucose inside the liposome and prior to its permeabilization.

At this stage, it is important to mention that all microscopic observations (both in PL and ECL) made during liposome membrane permeabilization are reproducible (see Electronic Supplementary Material Fig. S7 for another typical example among a dozen). In fact, the difficulty lies in quantifying luminescent signals which depends on the selected ROI. Unfortunately, our current approach does not allow a perfect isolation of a single liposome. The quantification of luminescent signals from a selected liposome is therefore often affected by luminescence generated by other liposomes located nearby. This was actually not the case for the liposome selected in Fig. 4a. Accordingly, and in parallel with the observations made in Fig. 4, the time-dependent evolution of PL and ECL intensities as well as the faradaic current for the liposome of interest could be plotted. The simultaneous evolution of the three signals is similar to that observed in the presence of authentic NADH. First, for $0 < t < 10$ s, PL intensity increases, in line with the arrival of the liposome at the electrode surface. The intensity then remains constant for ca. 10 s, indicating that the liposome has landed on the electrode surface and remains intact during this time. At $t = 20$ s, the PL signal intensity decreases (for around 20 s), indicating an "electro-permeabilization" of the liposome membrane. This permeabilization process releases some of the liposome content into the external environment, which can then be oxidized upon contact with the ITO surface. This electro-oxidation is asserted by the increase of both the amperometric and ECL signals.

Furthermore, it is noteworthy that the amperometric current obtained here is more intense than that observed with authentic encapsulated NADH (for the same co-enzyme concentration). This result may account for a more efficient leakage of the liposome studied here compared to the one loaded with authentic NADH.

Conclusion

In this work, we have primarily shown that NADH can be used as a biologically compatible ECL co-reactant to image membrane permeabilization events of giant liposomes. This was established not only in the presence of authentic NADH previously encapsulated inside

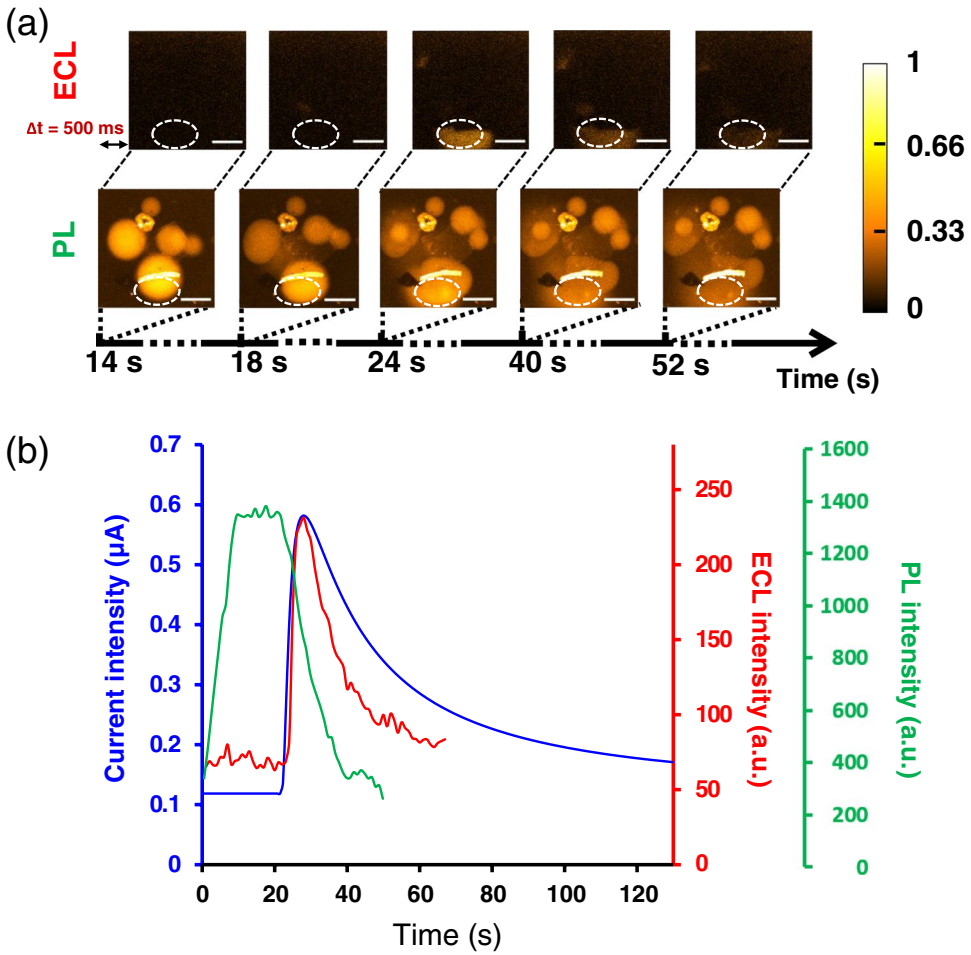

Fig. 4 **a** Parallel time-lapse imaging by ECL (top) and PL (below) showing the permeabilization of a liposome loaded with the ECL luminophore and enzymatic reagents. The liposome arriving at the surface of an ITO electrode polarized at a potential of + 1.2 V (vs. Ag/AgCl) initially contains NAD^+ (10^{-2} mol L^{-1}), $[Ru(bpy)_3]^{2+}$ ($2.5{\cdot}10^{-4}$ mol L^{-1}), GDH (80 U mL^{-1}), and glucose (0.35 mol L^{-1}). To avoid any overlap between both types of visual information, the ECL and PL images have an initial image acquisition time delay of 500 ms. The focus was made at the ITO electrode surface during the ECL and PL imaging. The dotted white circles in PL and ECL images represent the typical region of interest (ROI) taken into account for the quantitative analyses of the corresponding intensities. Scale bar: 100 µm. **b** Evolution of PL (green curve), ECL (red curve), and current (blue curve) signals obtained as a function of time for a single liposome (shown in **a**). Note: $t = 0$ s corresponds to the addition of liposomes in the electrochemical cell. The white line above the ROI is due to a dust on the electrode surface

liposomes, but also from its precursor NAD^+, assessing the completion of the GDH-promoted oxidation of glucose. On the one hand, considering the numerous reactions involving the NADH/NAD^+ couple, this work opens interesting perspectives in the imaging and post-analysis of metabolic processes in living cells or performed in artificial cells [77, 78]. On the other hand, our approach, which leads to the destruction of the lipid membrane is in line with the investigations of membrane permeabilization processes triggered by various stimuli including antimicrobial peptides [74].

Supplementary Information The online version contains supplementary material available at https://doi.org/10.1007/s00216-024-05133-y.

Acknowledgements F.B.T. thanks the doctoral school ED388 "Chimie Physique et de Chimie Analytique de Paris Centre" for a PhD grant.

Author contribution All authors contributed to the study conception, design, and analysis. The manuscript was written through contributions of all authors. All authors have given approval to the final version of the manuscript.

Funding This work was supported in parts by CNRS UMR 8640, Ecole Normale Supérieure, PSL University, and Sorbonne Université. N.S. received financial support from Agence Nationale de la Recherche (ELISE—ANR-21-CE42).

Declarations

Competing interests The authors declare no competing interests.

References

1. Blacker TS, Mann ZF, Gale JE, Ziegler M, Bain AJ, Szabadkai G, Duchen MR. Separating NADH and NADPH fluorescence in live cells and tissues using FLIM. Nat Commun. 2014;5:3936–44.
2. Park SY, Yoon SA, Cha Y, Lee MH. Recent advances in fluorescent probes for cellular antioxidants: Detection of NADH, hNQO1, H_2S, and other redox biomolecules. Coord Chem Rev. 2021;428: 213613.
3. Sun P, Zhang H, Sun Y, Liu J. The recent development of fluorescent probes for the detection of NADH and NADPH in living cells and in vivo. Spectrochim Acta A Mol Biomol Spectrosc. 2021;245: 118919.
4. Hung YP, Albeck JG, Tantama M, Yellen G. Imaging cytosolic NADH-NAD(+) redox state with a genetically encoded fluorescent biosensor. Cell Metab. 2011;14:545–54.
5. Zhao Y, Jin J, Hu Q, Zhou HM, Yi J, Yu Z, Xu L, Wang X, Yang Y, Loscalzo J. Genetically encoded fluorescent sensors for intracellular NADH detection. Cell Metab. 2011;14:555–66.
6. Xie W, Xu A, Yeung ES. Determination of NAD+ and NADH in a Single Cell under Hydrogen Peroxide Stress by Capillary Electrophoresis. Anal Chem. 2009;81:1280–4.
7. Yang H, Yang T, Baur JA, Perez E, Matsui T, Carmona JJ, Lamming DW, Souza-Pinto NC, Bohr VA. Nutrient-sensitive mitochondrial NAD+ levels dictate cell survival. Cell. 2007;130:1095–107.
8. Zhu S, Lei C, Sun J, Zhao X, Wang X, Yan X, Liu W, Wang H. Probing NAD+/NADH-dependent biocatalytic transformations based on oxidase mimics of MnO_2. Sens Actuators B. 2019;282:896–903.
9. Tao R, Zhao Y, Chu H, Wang A, Zhu J, Chen X, Zou Y, Shi M, Liu R, Su N, Du J, Zhou HM, Zhu L, Qian X, Liu H, Loscalzo J, Yang Y. Genetically encoded fluorescent sensors reveal dynamic regulation of NADPH metabolism. Nat Methods. 2017;14:720–8.
10. Gorton L, Domínguez E. Electrochemistry of NAD(P)+/NAD(P)H. In: Bard AJ (ed) Encyclopedia of Electrochemistry. Wiley. 2007. https://doi.org/10.1002/9783527610426.bard090004.
11. Radoi A, Compagnone D. Recent advances in NADH electrochemical sensing design. Bioelectrochemistry. 2009;76:126–34.
12. Moiroux J, Elving PJ. Effects of Adsorption, Electrode Material, and Operational Variables on the Oxidation of Dihydronicotinamide Adenine Dinucleotide at Carbon Electrodes. Anal Chem. 1978;50:1056–62.
13. Revenga-Parra M, Gómez-Anquela C, García-Mendiola T, Gonzalez E, Pariente F, Lorenzo E. Grafted Azure A modified electrodes as disposable β- nicotinamide adenine dinucleotide sensors. Anal Chim Acta. 2012;747:84–91.
14. Mano N, Thienpont A, Kuhn A. Adsorption and catalytic activity of trinitro- fluorenone derivatives towards NADH oxidation on different electrode materials. Electrochem Commun. 2001;3:585–9.
15. Maleki A, Nematollahi D, Clausmeyer J, Henig J, Plumeré N, Schuhmann W. Electrodeposition of catechol on glassy carbon electrode and its electrocatalytic activity toward NADH oxidation. Electroanalysis. 2012;24:1932–6.
16. Omar FS, Duraisamy N, Ramesh K, Ramesh S. Conducting polymer and its composite materials based electrochemical sensor for Nicotinamide Adenine Dinucleotide (NADH). Biosens Bioelectron. 2016;79:763–75.
17. Kumar SA, Chen SM. Electroanalysis of NADH Using Conducting and Redox Active Polymer/Carbon Nanotubes Modified Electrodes-A Review. Sensors. 2008;8:739–66.
18. Han S, Du T, Jiang H, Wang X. Synergistic effect of pyrroloquinoline quinone and graphene nano-interface for facile fabrication of sensitive NADH biosensor. Biosens Bioelectron. 2017;89:422–9.
19. del Barrio M, Rana M, Vilatela JJ, Lorenzo E, De Lacey AL, Pita M. Photoelectrocatalytic detection of NADH on n-type silicon semiconductors facilitated by carbon nanotube fibers. Electrochim Acta. 2021;377: 138071.
20. Bard AJ (ed). Electrogenerated Chemiluminescence (1st ed). CRC Press. 2004. https://doi.org/10.1201/9780203027011.
21. Gou X, Xing Z, Ma C, Zhu JJ. A Close Look at Mechanism, Application, and Opportunities of Electrochemiluminescence Microscopy. Chem Biomed Imaging. 2023;1:414–33.
22. Ma X, Gao W, Du F, Yuan F, Yu J, Guan Y, Sojic N, Xu G. Rational design of electrochemiluminescent devices. Acc Chem Res. 2021;54:2936–45.
23. Fiorani A, Han D, Jiang D, Fang D, Paolucci F, Sojic N, Valenti G. Spatially resolved electrochemiluminescence through a chemical lens. Chem Sci. 2020;11:10496–500.
24. Zanut A, Palomba F, Rossi Scota M, Rebeccani S, Marcaccio M, Genovese D, Rampazzo E, Valenti G, Paolucci F, Prodi L. Dye-Doped Silica Nanoparticles for Enhanced ECL-Based Immunoassay Analytical Performance. Angew Chem Int Ed. 2020;59:21858–63.
25. Du F, Chen Y, Meng C, Lou B, Zhang W, Xu G. Recent advances in electrochemiluminescence immunoassay based on multiple-signal strategy. Curr Opin Electrochem. 2021;28: 100725.
26. Dutta P, Han D, Goudeau B, Jiang D, Fang D, Sojic N. Reactivity mapping of luminescence in space: insights into heterogeneous electrochemiluminescence bioassays. Biosens Bioelectron. 2020;165: 112372.
27. Zhang J, Arbault S, Sojic N, Jiang D. Electrochemiluminescence Imaging for Bioanalysis. Annu Rev Anal Chem. 2019;12:275–95.
28. Rebeccani S, Zanut A, Santo CI, Valenti G, Paolucci F. A Guide Inside Electrochemiluminescent Microscopy Mechanisms for Analytical Performance Improvement. Anal Chem. 2022;94:336–48.
29. Zhao W, Chen HY, Xu JJ. Electrogenerated chemiluminescence detection of single entities. Chem Sci. 2021;12:5720–36.
30 Meng C, Knežević S, Du F, Guan Y, Kanoufi F, Sojic N, Xu G. Recent advances in electrochemiluminescence imaging analysis. eScience. 2022;2:591–605.
31. Wilson AJ, Marchuk K, Willets KA. Imaging Electrogenerated Chemiluminescence at Single Gold Nanowire Electrodes. Nano Lett. 2015;15:6110–5.
32. Dick JE, Renault C, Kim BK, Bard AJ. Simultaneous Detection of Single Attoliter Droplet Collisions by Electrochemical and Electrogenerated Chemiluminescent Responses. Angew Chem Int Ed. 2014;53:11859–62.
33. Fan FRF, Park S, Zhu Y, Ruoff RS, Bard AJ. Electrogenerated Chemiluminescence of Partially Oxidized Highly Oriented Pyrolytic Graphite Surfaces and of Graphene Oxide Nanoparticles. J Am Chem Soc. 2009;131:937–9.
34. Zhu MJ, Pan JB, Wu ZQ, Gao XY, Zhao W, Xia XH, Xu JJ, Chen HY. Electrogenerated Chemiluminescence Imaging of Electrocatalysis at a Single Au-Pt Janus Nanoparticle. Angew Chem Int Ed. 2018;57:4010–4.
35. Sentic M, Milutinovic M, Kanoufi F, Manojlovic D, Arbault S, Sojic N. Mapping electrogenerated chemiluminescence reactivity in space: mechanistic insight into model systems used in immunoassays. Chem Sci. 2014;5:2568–72.
36. Deiss F, LaFratta CN, Symer M, Blicharz TM, Sojic N, Walt DR. Multiplexed Sandwich Immunoassays Using Electrochemiluminescence Imaging Resolved at the Single Bead Level. J Am Chem Soc. 2009;131:6088–9.
37. Valenti G, Zangheri M, Sansaloni SE, Mirasoli M, Penicaud A, Roda A, Paolucci F. Transparent Carbon Nanotube Network

for Efficient Electrochemiluminescence Devices. Chem Eur J. 2015;21:12640–5.
38. Xu J, Huang P, Qin Y, Jiang D, Chen HY. Analysis of Intracellular Glucose at Single Cells Using Electrochemiluminescence Imaging. Anal Chem. 2016;88:4609–12.
39. Zhou J, Ma G, Chen Y, Fang D, Jiang D, Chen HY. Electrochemiluminescence Imaging for Parallel Single-Cell Analysis of Active Membrane Cholesterol. Anal Chem. 2015;87:8138–43.
40. Ma GZ, Zhou JY, Tian CX, Jiang DC, Fang DJ, Chen HY. Luminol Electrochemiluminescence for the Analysis of Active Cholesterol at the Plasma Membrane in Single Mammalian Cells. Anal Chem. 2013;85:3912–7.
41. Liu G, Ma C, Jin BK, Chen ZX, Zhu JJ. Direct Electrochemiluminescence Imaging of a Single Cell on a Chitosan Film Modified Electrode. Anal Chem. 2018;90:4801–6.
42 Valenti G, Scarabino S, Goudeau B, Lesch A, Jović M, Villani E, Sentic M, Rapino S, Arbault S, Paolucci F, Sojic N. Single Cell Electrochemiluminescence Imaging: From the Proof-of-Concept to Disposable Device-Based Analysis. J Am Chem Soc. 2017;139:16830–7.
43. Voci S, Goudeau B, Valenti G, Lesch A, Jović M, Rapino S, Paolucci F, Arbault S, Sojic N. Surface-Confined Electrochemiluminescence Microscopy of Cell Membranes. J Am Chem Soc. 2018;140:14753–60.
44. Ma Y, Colin C, Descamps J, Arbault S, Sojic N. Shadow Electrochemiluminescence Microscopy of Single Mitochondria. Angew Chem Int Ed. 2021;60:18742–9.
45. Ding L, Zhou P, Yan Y, Su B. Electrochemiluminescence Imaging of Cellular Contact Guidance on Microfabricated Substrates. Chem Biomed Imaging. 2023;1:558–65.
46. Guo M, Du D, Wang J, Ma Y, Yang D, Haghighatbin MA, Shu J, Nie W, Zhang R, Bian Z, Wang L, Smith ZJ, Cui H. Three-Biomarker Joint Strategy for Early and Accurate Diagnosis of Acute Myocardial Infarction via a Multiplex Electrochemiluminescence Immunoarray Coupled with Robust Machine Learning. Chem Biomed Imaging. 2023;1:179–85.
47. Deng L, Zhang L, Shang L, Guo S, Wen D, Wang F, Dong S. Electrochemiluminescence detection of NADH and ethanol based on partial sulfonation of sol–gel network with gold nanoparticles. Biosens Bioelectron. 2009;24:2273–6.
48. Devadoss A, Dennany L, Dickinson C, Keyes TE, Forster RJ. Highly sensitive detection of NADH using electrochemiluminescent nanocomposites. Electrochem Commun. 2012;19:43–5.
49. Sentic M, Arbault S, Goudeau B, Manojlovic D, Kuhn A, Bouffier L, Sojic N. Electrochemiluminescent swimmers for dynamic enzymatic sensing. Chem Comm. 2014;50:10202–5.
50. Chen HJ, Liu X, Yin C, Li W, Qin XD, Chen CY. A dual-signal output ratiometric electrochemiluminescent sensor for NADH detection. Analyst. 2019;144:5215–22.
51. Michelraj S, Raju CV, Lakshminarasimhan N, Kumar SS. Electrogenerated chemiluminescence of phosphate-modified polymeric carbon nitride for sensing of NADH: role of luminophore-coreactant interactions in enhancing the signal. J Electrochem Soc. 2019;166:H565–72.
52. Zhang B, Shi S, Shi W, Sun Z, Kong X, Wei M, Duan X. Assembly of ruthenium (II) complex/layered double hydroxide ultrathin film and its application as an ultrasensitive electrochemiluminescence sensor. Electrochim Acta. 2012;67:133–9.
53. Qian J, Wang K, Jin YC, Yang XW, Jiang L, Yan YT, Dong XY, Li HM, Qiu BJ. Polyoxometalate@ magnetic graphene as versatile immobilization matrix of Ru(bpy)(3)(2+) for sensitive magneto-controlled electrochemiluminescence sensor and its application in biosensing. Biosens Bioelectron. 2014;57:149–56.
54. Zhuang Y, Ju H. Determination of Reduced Nicotinamide Adenine Dinucleotide Based on Immobilization of Tris(2,2′-bipyridyl) Ruthenium(II) in Multiwall Carbon Nanotubes/Nafion Composite Membrane. Anal Lett. 2005;38:2077–88.
55. Li YL, Yang XR, Yang F, Wang YP, Zheng PH, Liu XX. Effective immobilization of Ru(bpy)32+ by functional composite phosphomolybdic acid anion on an electrode surface for solid-state electrochemiluminescene to sensitive determination of NADH. Electrochim Acta. 2012;66:188–92.
56. Chovin A, Garrigue P, Sojic N. Remote NADH imaging through an ordered array of electrochemiluminescent nanoapertures. Bioelectrochemistry. 2006;69:25–33.
57. Delaney JL, Hogan CF, Tian J, Shen W. Electrogenerated Chemiluminescence Detection in Paper-Based Microfluidic Sensors. Anal Chem. 2011;83:1300–6.
58. Jin ES, Norris BJ, Pantano P. An electrogenerated chemiluminescence imaging fiber electrode chemical sensor for NADH. Electroanalysis. 2001;13:1287–90.
59. Ferraraccio LS, Bertoncello P. Electrochemiluminescence (ECL) biosensor based on tris(2,2′-bipyridyl) ruthenium(II) with glucose and lactate dehydrogenases encapsulated within alginate hydrogels. Bioelectrochemistry. 2023;150: 108365.
60. Jameison F, Sanchez RI, Dong L, Leland JK, Yost D, Martin MT. Electrochemiluminescence-Based Quantitation of Classical Clinical Chemistry Analytes. Anal Chem. 1996;68:1298–302.
61. Waseem A, Yaqoob M, Nabi A, Greenway GM. Determination of Thyroxine Using Tris(2,20-Bipyridyl)Ruthenium(III)-NADH Enhanced Electrochemiluminescence Detection. Anal Lett. 2007;40:1071–83.
62. Milutinovic M, Sallard S, Manojlovic D, Mano N, Sojic N. Glucose sensing by electrogenerated chemiluminescence of glucose-dehydrogenase produced NADH on electrodeposited redox hydrogel. Bioelectrochemistry. 2011;82:63–8.
63. Lei R, Wang XY, Zhu SF, Li N. A novel electrochemiluminescence glucose biosensor based on alcohol-free mesoporous molecular sieve silica modified electrode. Sens Actuators B Chem. 2011;158:124–9.
64. Wang GJ, Jin F, Dai N, Zhong ZY, Qing Y, Li MX, Yuan R, Wang D. Signal-enhanced electrochemiluminescence immunosensor based on synergistic catalysis of nicotinamide adenine dinucleotide hydride and silver nanoparticles. Anal Biochem. 2012;422:7–13.
65. Lin X, Wang QH, Zhu S, Xu JJ, Xia Q, Fu YZ. A highly sensitive glutamic acid biosensor based on the determination of NADH enzymically generated by L-glutamic dehydrogenase. RSC Adv. 2016;6:45829–34.
66. de Poulpiquet A, Diez-Buitrago B, Milutinovic MD, Sentic M, Arbault S, Bouffier L, Kuhn A, Sojic N. Dual Enzymatic Detection by Bulk Electrogenerated Chemiluminescence. Anal Chem. 2016;88:6585–92.
67. Dimova R. Giant Vesicles and Their Use in Assays for Assessing Membrane Phase State, Curvature, Mechanics, and Electrical Properties. Annu Rev Biophys. 2019;48:93–119.
68. Toyota T, Zhang Y. Identifying and Manipulating Giant Vesicles: Review of Recent Approaches. Micromachines. 2022;13:644.
69. Menger FM, Keiper JS. Chemistry and physics of plant vesicles as biomembrane models. Curr Opin Chem Biol. 1998;2:726–32.
70. Dobereiner HG. Properties of giant vesicles. Curr Opin Colloid Interface Sci. 2000;5:256–63.
71. Messina P, Lemaitre F, Huet F, Ngo KA, Vivier V, Labbé E, Buriez O, Amatore C. Monitoring and Quantifying the Passive Transport of Molecules Through Patch-Clamp Suspended Real and Model Cell Membranes. Angew Chem Int Ed. 2014;53:3192–6.
72 Perez Jimenez AI, Challier L, Ait-Yahiatène E, Delacotte J, Labbé E, Buriez O. Selective Electrochemical Bleaching of the Outer Leaflet of Fluorescently Labeled Giant Liposomes. Chem Eur J. 2017;23:6781–7.

73. Ben Trad F, Wieczny V, Delacotte J, Morel M, Guille-Collignon M, Arbault S, Lemaitre F, Sojic N, Labbé E, Buriez O. Dynamic Electrochemiluminescence Imaging of Single Giant Liposome Opening at Polarized Electrodes. Anal Chem. 2022;94:1686–96.
74. Ben Trad F, Delacotte J, Guille-Collignon M, Lemaitre F, Arbault S, Sojic N, Burlina F, Labbé E, Buriez O. Electrochemiluminescence Imaging of Liposome Permeabilization by an Antimicrobial Peptide: Melittin. Chem Biomed Imaging. 2023;1:58–65.
75. Downey TM, Nieman TA. Chemiluminescence Detection Using Regenerable Tris(2,2'-Bipyridyl)Ruthenium(II) Immobilized in Nafion. Anal Chem. 1992;64:261–8.
76. Martin AF, Nieman TA. Glucose Quantitation Using an Immobilized Glucose-Dehydrogenase enzyme reactor and a Tris(2,2'-Bipyridyl)Ruthenium(II) Chemiluminescent Sensor. Anal Chim Acta. 1993;281:475–81.
77. Lefrançois P, Santolini J, Arbault S. Electroanalysis at a Single Giant Vesicle Generating Enzymatically a Reactive Oxygen Species. Anal Chem. 2021;93:13143–51.
78. Robinson T. Microfluidic Handling and Analysis of Giant Vesicles for Use as Artificial Cells: A Review. Adv Biosys. 2019;3:1800318.